

Advances in Magnetized Plasma Propulsion and Radiation Shielding

Robert Winglee

Department of Earth and Space Sciences
University of Washington, Seattle WA 98195-1310
winglee@ess.washington.edu

Abstract

Mini-magnetosphere, that is magnetic field inflated by the injection of plasma have several applications key to the exploration of space, including radiation shielding and augmentation of spacecraft thrust through momentum coupling with the solar wind. The systems are important because this inflation can be done without large mechanical structures and as such represent an example of a transformable technology. This paper uses multi-fluid simulations to detail the physics behind the inflation and the requirements to produce deflection of solar wind and other energetic particles. It is shown that the inflation itself is associated with the formation of a diamagnetic cavity that produces the rearrangement of the magnetic field both in front of and behind the magnet, and that this rearrangement greatly enhances the ability of the system to deflect charged particles in the forward direction. The solar wind adds momentum into the system to produce a 100:1 leverage on the thrust of the system, and adds energy to increase the magnetic field energy density so that is able to deflect energetic particles is further increased above what the mini-magnetosphere can do alone. Radiation shielding of GeV particles then becomes possible at 100's kW power levels.

1. Introduction

Space is filled with energetic plasma. This plasma has three components. From the perspective of total mass density, the dominant component is the solar wind which at 1 AU has a typical density of about $4\text{--}6\text{ cm}^{-3}$ and speed of $\sim 400\text{--}800\text{ km/s}$. Several orders down in density but several orders higher at MeV energy levels are the solar energetic particles (SEP) that are associated with solar flare activity. At still higher energy and less density are the galactic cosmic rays (GCR) at GeV energies/nucleon.

This plasma environment has an important influence on the exploration of space. First, it provides a severe radiation hazard for human exploration and to sensitive scientific instrumentation. At the same time it represents a huge source of energy. It is sufficient for example to produce differential erosion of surface material of Ganymede¹ and for the erosion of the Martian atmosphere². At the same time there is potential for harnessing the solar wind for enhanced spacecraft propulsion, as suggested in Mini-Magnetospheric Plasma Propulsion (M2P2)^{3,4}. In this scheme a magnetic field attached to the spacecraft is expanded by the injection of plasma to a scale size of the order of 10 km. The magnetic fields associated with supporting the mini-magnetosphere produce the deflection of the solar wind, with the exchange of momentum being carried to the spacecraft via the magnetic field lines. In so doing a leverage in momentum of nearly a factor of 100 can be obtained. Larger mini-magnetospheres have the potential for providing shielding from SEPs and GCR. Combination of the propulsion and radiation systems would mean that no dead mass has to be carried into space in order to produce the shielding. As such this technology is transformable in both its ability to shape the magnetic field and its effective shielding, as well as its application from spacecraft propulsion to spacecraft shielding.

In this paper we detail for the first time the dynamics of the expansion of mini-magnetosphere with the inclusion of finite ion cyclotron processes. Ion cyclotron effects are important as they produce azimuthal effects that produce an angled or twisted mini-magnetosphere. This angling of the plasma flow within the mini-magnetosphere is consistent with laboratory experiments where the peak plasma density is seen to angle away from the vacuum magnetic field⁵. These ion cyclotron effects are also important for propulsion applications where the same ion cyclotron effects will produce angular deflection of solar wind

particles leading to not just radial thrust but significant azimuthal thrust.

The requirements for deflection of plasma from a mini-magnetosphere are discussed in Section 2. Details of the simulation model are then given in Section 3. Results for magnetic plasma expansion are presented in Section 4 and deflection of the solar wind in Section 5. A summary of results is given in Section 6.

2. Magnetic Field Requirements

In order for a magnetic field to deflect a charged particle, the scale length of the magnetic field within the mini-magnetosphere has to be comparable to the gyro-radius of the particle, i.e.

$$v_{\perp, \text{deflect}} \leq \frac{q}{m} \int \mathbf{B}_{\perp} dr \quad (1)$$

where q is the charge of the particle, m is the relativistic mass, and the subscript \perp denotes quantities perpendicular to the magnetic field. Any particle with $v_{\perp} < v_{\perp, \text{dipole}}$ will be deflected, irrespective of its initial pitch angle. For shielding of MeV protons and < 10 MeV electrons, (1) then requires that $\int \mathbf{B}_{\perp} dr$ be of the order of 0.03 Tesla meter (Tm). Deflection of GeV would then require $\int \mathbf{B}_{\perp} dr$ to be of the order of 1 Tm while solar wind particles require 0.001 Tm. This criterion can also be verified by standard single particle tracking techniques.

Now suppose that the magnetic field has a falloff of the form $1/r^n$, where $n=3$ for a dipole and $n<3$ if the magnetic field has been stretched by plasma convection. In this case (1) reduces to

$$v_{\perp, \text{deflect}} \approx \frac{q}{m} \frac{B_0 R_m}{n-1} \quad \text{for } n < 1 \quad (2a)$$

$$v_{\perp, \text{deflect}} \approx \frac{q}{m} B_0 R_m \ln\left(\frac{L}{R_m}\right) \quad \text{for } n = 1 \quad (2b)$$

where R_m is the magnet radius, B_0 is the field strength at the equator of the magnet and L is the size of the mini-magnetosphere. For example, for a simple dipole, the magnetic field falls off as r^{-3} and (2a) reduces to $v_{\perp, \text{dipole}} \sim (q/m) B_0 R_m/2$. By stretching the magnetic field to something that falls off with $n=2$, particles with velocities twice as high as $v_{\perp, \text{dipole}}$ can be deflected, i.e. $v_{\perp, \text{deflect}} = 2 v_{\perp, \text{dipole}}$. And if one were to achieve a falloff of the order of $n=1$ then depending on L/R_m , factors of 10 (e.g. $R_m = 20\text{cm}$ and $L = 30\text{ m}$) to 20 (e.g. $R_m = 20\text{cm}$ and $L = 20\text{ km}$) increases in $v_{\perp, \text{deflect}}$ can be achieved. In other words there can be massive savings in the magnet requirements if the magnetic field can be inflated to have a slower falloff than the initial dipole.

There are two unresolved issues with mini-magnetospheres. First, how does one produce such a

magnetic field configuration and second how much thrust if any is generated on the spacecraft by the deflection of energetic particles.

To answer these questions in detail we will use the simulations described in the next section. It is important to note at the outset though that a $1/r$ falloff in the magnetic field cannot be accomplished in all directions by the spacecraft itself as it would require too much energy. We will demonstrate that the plasma injection produces an equatorial current sheet that generates a falloff in the magnetic field approaching $1/r$. This slow falloff is achieved by a reduction in field strength near the magnet, and the integral of B is actually relatively low in equator of the mini-magnetosphere. In other directions through the field falloff is faster at $\sim 1/r^{1.7}$ with the total increase in the integral of B being about a factor of 10 above the initial dipole. The observed falloffs become slower when the forcing of the solar wind is taken into account. This forcing increases the magnetic field energy density within the mini-magnetosphere, and also imparts momentum to the mini-magnetosphere to produce a leverage of thrust.

3. Simulation Model

To quantitatively demonstrate how the inflation of the mini-magnetosphere occurs, we use 3-D multi-fluid simulations that incorporate the ion cyclotron effects in the fluid dynamics and in the induction equation. This code is based on extensive modeling of the terrestrial magnetosphere [e.g. *Winglee, 2000; Winglee et al., 2002*]. Within the code, the dynamics of each component is given by

$$\frac{\partial \rho_{\alpha}}{\partial t} + \nabla \cdot (\rho_{\alpha} \mathbf{V}_{\alpha}) = 0 \quad (3)$$

$$\rho_{\alpha} \frac{d\mathbf{V}_{\alpha}}{dt} = q_{\alpha} n_{\alpha} (\mathbf{E}_{\alpha} + \mathbf{V}_{\alpha} \times \mathbf{B}(\mathbf{r})) - \nabla P_{\alpha} \quad (4)$$

$$\frac{\partial P_{\alpha}}{\partial t} = -\gamma \nabla \cdot (P_{\alpha} \mathbf{V}_{\alpha}) + (\gamma - 1) \mathbf{V}_{\alpha} \cdot \nabla P_{\alpha} \quad (5)$$

MHD is based on combining the above equations to give a single-fluid treatment. Our multi-fluid treatment is based on the same equations, but the dynamics of the electrons and the different ion species are kept separate. For electrons, it is assumed that they have sufficiently high mobility along the field lines that they are approximately in steady-state drift motion. In other words, their motion can be described by drift motion (i.e. $d\mathbf{V}_{de}/dt = 0$) so that (3) for the electrons reduces to

$$\mathbf{E} + \mathbf{V}_{de} \times \mathbf{B} + \frac{1}{en_e} \nabla P_e = 0 \quad (6)$$

Equation (6) is solved by writing V_{de} in terms of ion velocity and the induced currents assuming quasi-neutrality, i.e.,

$$n_e = \sum_i n_i, V_{de} = \sum_i \frac{n_i}{n_e} V_i - \frac{\mathbf{J}}{en_e}, \mathbf{J} = \frac{1}{\mu_0} \nabla \times \mathbf{B} \quad (7)$$

where the sum of i is over the different ion species that may be present (for example if there is break down of a molecular gas or impurities generated by sputtering). Substitution of (7) into (6) yields the modified Ohm's law of

$$\mathbf{E} = - \sum_i \frac{n_i}{n_e} \mathbf{V}_i \times \mathbf{B} + \mathbf{J} \times \mathbf{B} + \frac{1}{en_e} \nabla P_e + \eta(\mathbf{x}) \mathbf{J} \quad (8)$$

The first term in (8) is the ideal Ohm's law, while the second and third terms given the Hall and ∇P corrections (both of which are of order of the ion skin depth relative to the scale length of the system) and the last term $\eta(\mathbf{x}) \mathbf{J}$ is added to allow for finite conductivity regions within the magnet and associated neutral plume near the injection region. Collisions beyond this region are assumed to be negligible. No anomalous resistivity is included as the non-ideal terms included in (8) are sufficient to give a full accounting of ion cyclotron terms that drive much of the dissipative processes.

The description of the electron dynamics is completed by the pressure equation

$$\frac{\partial P_e}{\partial t} = -\gamma \nabla \cdot (P_e \mathbf{V}_{de}) + (\gamma - 1) \mathbf{V}_{de} \cdot \nabla P_e \quad (9)$$

and the evolution of the magnetic field by the induction equation

$$\frac{\partial \mathbf{B}}{\partial t} + \nabla \times \mathbf{E} = 0 \quad (10)$$

The ion dynamics is determined by time stepping for each individual ion species equations (3)-(5) using the electric field in (8). Note that due to the presence of different ion species, the bulk speed of an individual ion component \mathbf{V}_α does not have to equal the average drift speed of all the ion components (i.e. $\Sigma(n_i \mathbf{V}_i)/n_e$ terms) as assumed in MHD, and this difference sets up the various ion cyclotron effects within the different ion species.

The above equations are solved using a two-step Lax-Wendroff differencing scheme [Richtmyer and Morton, 1967] with Lapidus smoothing on plasma properties only [Sod, 1978]. The latter is required to remove unphysical grid point oscillations across sharp discontinuities such as the bow shock as well as the grid point growth of non-physical whistlers. While the two-step Lax-Wendroff scheme is one of the simpler numerical methods, its simplicity allows a tractable

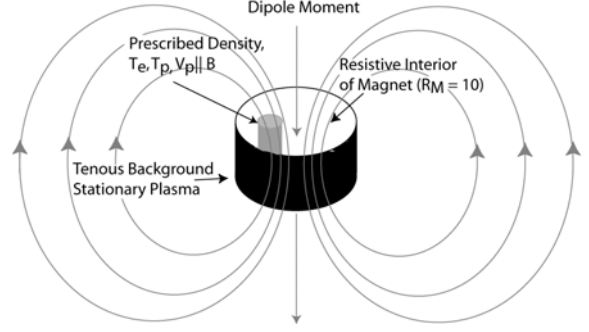


Figure 1. Schematic of the set up of the inner boundary of the simulations system. There is no convective electric field at the boundary conditions so that there is no artificial injection of magnetic flux into the system.

means for including much more complicated but more realistic physics associated with the above multi-fluid treatment. The equations are solved on a structured Cartesian grid using a box-in-box grid system. This system allows us to zoom down to the surface of the magnet at 2.5 cm resolution, or zoom out to several km to image the full inflation of the system.

The set up of the simulations at the inner boundary is shown in Figure 1, and closely models the actual laboratory kW prototype^{4,5}. A dipole magnet represented by a hollow (black/white) cylinder with a radius of 20 cm. The field strength at the top of the magnet is set at 2 kG. The plasma is injected from the gray cylinder within the magnet with a radius of 2.5 cm (presenting the plasma source) with a density of $6 \times 10^{11} \text{ cm}^{-3}$, and a speed of 20 km/s. This corresponds to a source of 30 mN of thrust. Standard plasma thrusters typically produce about 40 mN/kW so that the parameters assumed here are consistent with only a kW system. Higher performance can be attained by using scaling the system to the high powers will be available in future missions such as the Jupiter Icy Moon Orbiter which will have a power 100's kW.

4. Magnetic Field Inflation

In the original description of M2P2, the expansion of the magnetic field was done simultaneously in the presence of the solar wind. This allowed the equilibrium size of the system to be determined accurately, but masked the physical processes that enable the mini-magnetosphere to first inflate, and how energy from the solar wind is couple into the mini-magnetosphere to produce thrust. To remove such ambiguities we first model the inflation of the mini-magnetosphere which is illustrated in Figure 2 which

shows the evolution of the magnetic field lines in the near proximity to the magnet.

The magnet position is indicated by the grey cylinder, and mapping through a few fixed points have been highlighted in black. At early times (Figure 4b) the plasma has had insufficient time to reach the equator so the field lines are pulled upwards and have a squared appearance. As the flux tubes become filled with plasma and move outward, they develop a more oval or stretched appearance (Figures 2c, and 2d). This stretching of the field lines is simulation to previous Hall-MHD simulations^{3,4} and the main effect of the ion cyclotron terms included here is to produce a twist to the left on the field lines.

Note also that the back field lines are also affected by the plasma injection, albeit on a delayed time scale (Figures 2c and 2d). Essentially the plasma injection sets up a global convection pattern, drawing magnetic flux left behind into the void produced by the outward convection of plasma and magnetic field on the front side of the magnet. This convection then leads to the collapse of the magnetic field behind the magnet.

The corresponding change in the magnetic field intensity is shown in Figure 3. First and foremost note that there is essentially no change in the magnetic field strength above the magnet, i.e. there is no injection of magnetic flux into the system. Second the initial

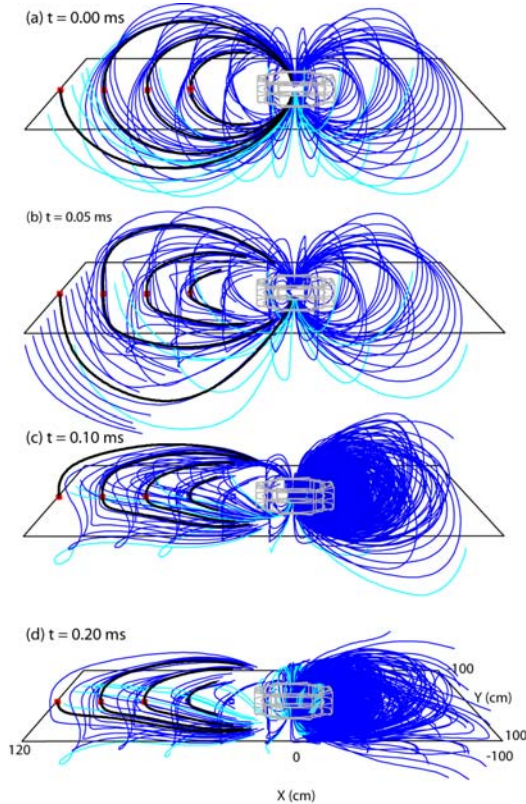


Figure 2. Evolution of the magnetic field lines under plasma inflation.

change in the magnetic field occurs in the region of outward moving plasma in front of the magnet. The regions in front of the expanding plasma are compressed and this leads to a local increase in the magnetic field. Behind this expansion wave, a diamagnetic cavity forms in the equatorial region that leads to a local minimum in the field at the equator and enhanced field above the equator.

An alternative way to think about these magnetic perturbations is that an equatorial current sheet is being formed. This current sheet is associated with weak fields in the current sheet itself but produces enhanced magnetic field above and below it as seen in the Figure 3. Note that because the injection is only in the forward direction the current does not close azimuthally, but rather closes at high latitudes, similar to the terrestrial current sheet. As the plasma and associated current sheet expand outwards the diamagnetic region increases around the flanks (Figure 3c), and the magnetic field behind the magnet is weakened (Figure 3d).

As noted in Section 2 the plasma expansion and associated convection of magnetic field will produce a slower falloff in the magnetic field as already seen in Figure 3. The issue is then what is happening to the magnetic flux in the system. This issue is addressed in Figure 4, which shows contours of B_z . The values of B_z is limited so that one can clearly identify regions of positive B_z (gray regions) and negative B_z (white). Integration of B_z indicates that magnetic flux is conserved in the simulation to within numerical error. The conservation of flux though means that as the magnetic field expands outward, regions of negative B_z must develop in the equatorial region and do so as seen in Figure 4b-d. The size of the negative region grows

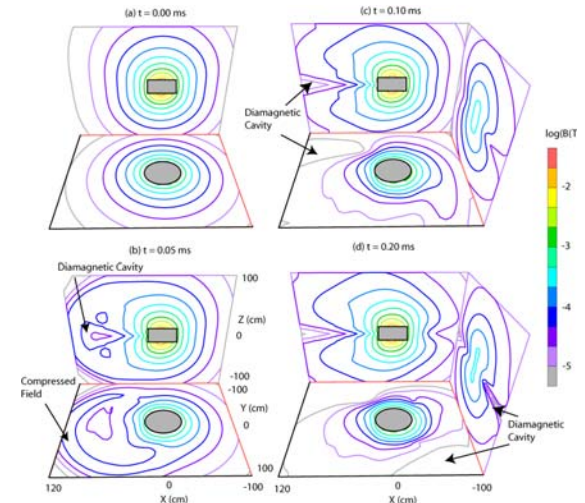


Figure 3. Evolution of the magnetic field intensity corresponding to Figure 2. Contours are in the equatorial plane (bottom), x-z plane in the middle (back), and y-z plane (at the right panel)

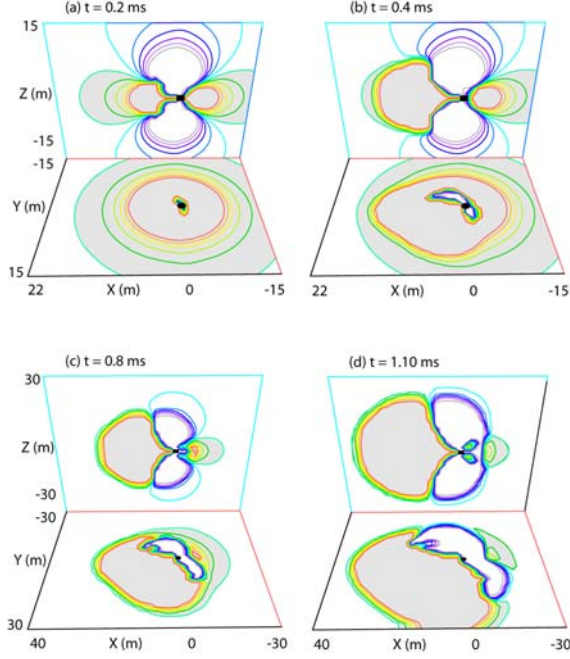


Figure 4. Evolution of the B_z in the equatorial and x-z planes. Positive (negative) B_z is shaded in gray (white). The scale sizes changes for the later times to match the expansion of the magnetic field.

in a self-similar fashion along with the positive B_z region (Figure 4c and 4d).

The reason for this negative B_z region is simple. An equatorial current is being generated by the injected plasma. Because of finite ion cyclotron effects the direction of the current sheet is not exactly orthogonal

to the injection direction. The direction of the current sheet is basically parallel to the line of transition between the negative and positive B_z regions in the equator. Because this current system is very much larger than the original magnet, its magnetic field dominates that of the magnet and the regions behind the injection region eventually develop a negative B_z while in front there expanding positive B_z .

The presence of negative B_z means that the magnetic field in these regions do not map into the magnet, only a subset of the positive regions are connected to the magnet. This is not a problem as it is the forward field lines that do the deflection and not the rear field regions. The critical point is that while the magnetic field structure is probably more complicated that one would like, it behaves exactly as expected with the initial magnet and plasma injection being able to create a very large current system in space.

Greater detail into the form of the magnetic field can be seen in Figure 5, which shows the line cuts in the forward direction at 0° and 45° elevation. As already seen in Figure 2, the expansion of the magnetic field produces a diamagnetic cavity in the equatorial plane which is seen in Figure 5a as the field strength near the magnet falling below its initial dipole value. The compression of flux tubes as the plasma expands outward is seen as the peak in field strength at the leading edge of the magnetic perturbations. Behind this peak the average falloff in the magnetic field strength is sustained at about $R^{-1.2}$ over two orders of magnitude distances beyond the original magnet, consistent with initial studies.

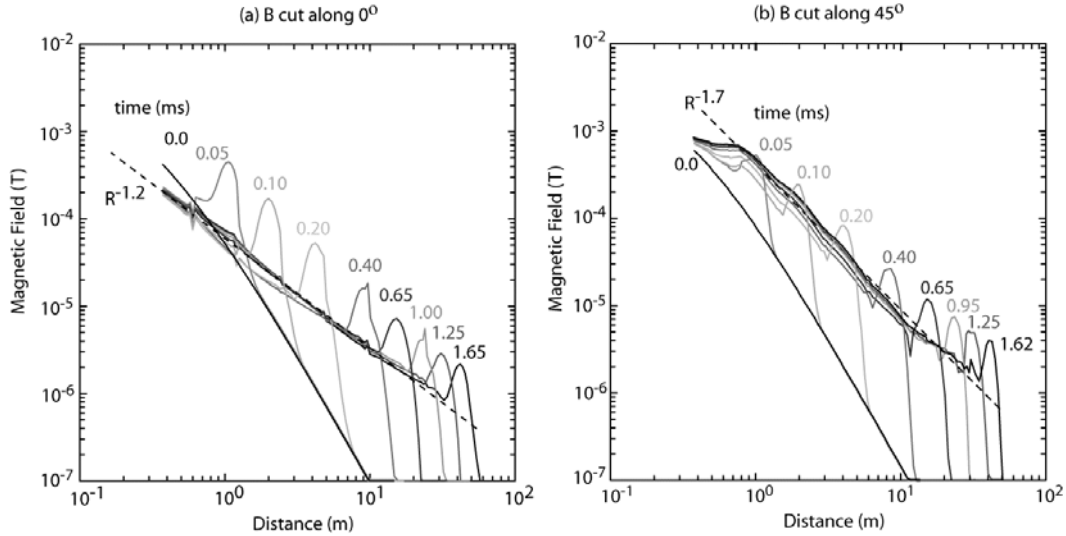


Figure 5. Cuts in the magnetic field strength as a function of radial distance forward ($x > 0$) of the magnet at (a) 0° (equatorial plane) and (b) 45° elevation. The heavy line at $t=0$ has a falloff as R^{-3} and the dashed line shows the fitted slope at later times.

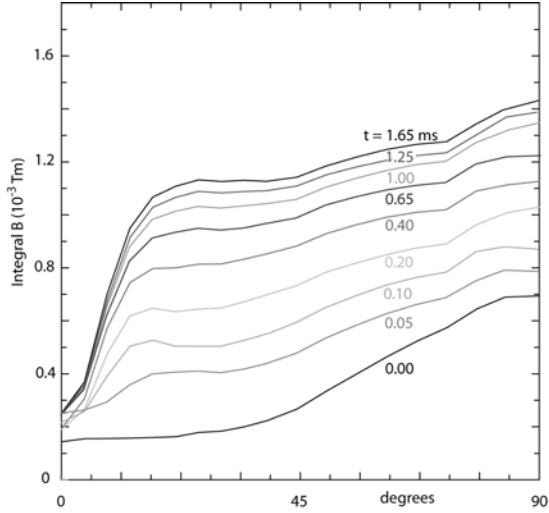


Figure 6. Integral of B at different angles of elevation in the forward direction.

The actual slope in these expansion experiments is determined by the ratio of the plasma flow speed to Alfvén speed which is set at $1/8$. Slower speeds are subject to faster falloffs and higher speeds can drive the falloff closer to R^{-1} .

Note that out of the equatorial plane, the falloff in the field strength is significantly different as seen in Figure 5b. Since line cuts are taken at 45° they are above the diamagnetic cavity. Thus the magnetic field strength close to the magnet increases above the initial level, being a constructive summation of the dipole field strength with that from the equatorial current system. The fall off however is steeper at $R^{-1.7}$. This means that the magnetic field energy density is increasing at a rate that can be supported by the plasma injection and that unphysical increases in the magnetic

field energy is not occurring.

As measure of the ability of the mini-magnetosphere to deflect plasma, Figure 6 shows the integral of the magnetic field strength along radial paths into the magnet at various angles of elevation. Because of the diamagnetic cavity there is only a small increase in magnetic field strength in the equatorial (low elevation) region. Above about 22° the field strength increase by a factor of about 8, consistent with the estimates given in Section 2 for various magnetic field falloffs.

It can also be seen in Figure 6 that the highest rate of increase in integral of B occurs at early times. This saturation of the growth rate of growth occurs because the contributions from large distances become increasingly small. Note that if there was an artificial injection of flux occurring one would expect the rate to increase monotonically, which is clearly not happening.

5. Solar Wind Deflection

As discussed in Section 2, an integral B of 0.001 is required to deflect solar wind particles. It is seen from Figure 6 that while the initial magnet is insufficient to perform such deflection, the inflated system is. This section focuses on ability of the mini-magnetosphere to deflect an external plasma wind, and the transfer of energy and moment from this wind into the mini-magnetosphere. To keep the simulations feasible we use a speed of 300 km/s and an enhanced proton density of $5 \times 10^6 \text{ cm}^{-3}$. The actual density is not a key parameter in the sense that the size of the magnetosphere is determined by pressure balance

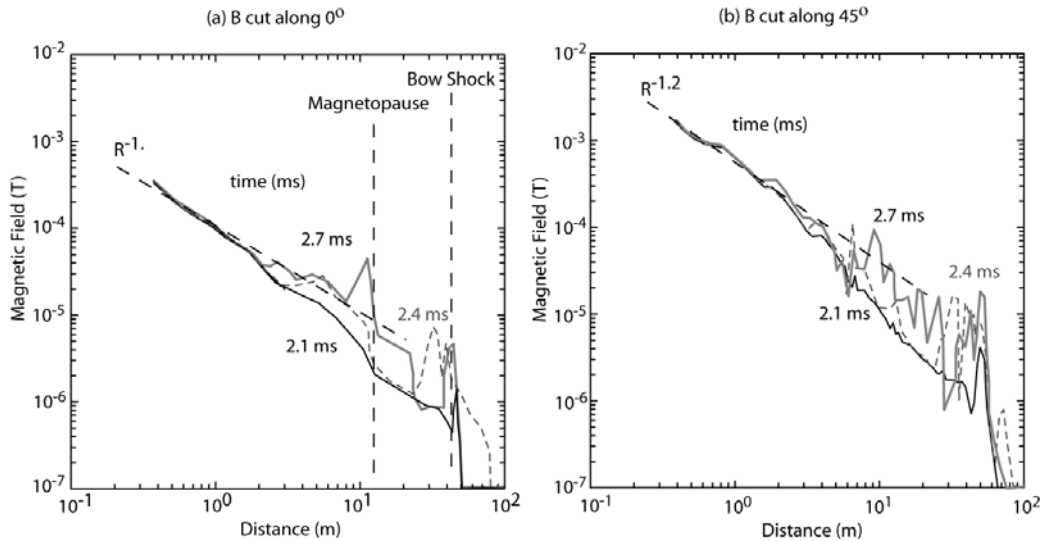


Figure 7. Continuation of Figure 5 with the solar wind arriving at the mini-magnetosphere at $t = 2.1$ ms.

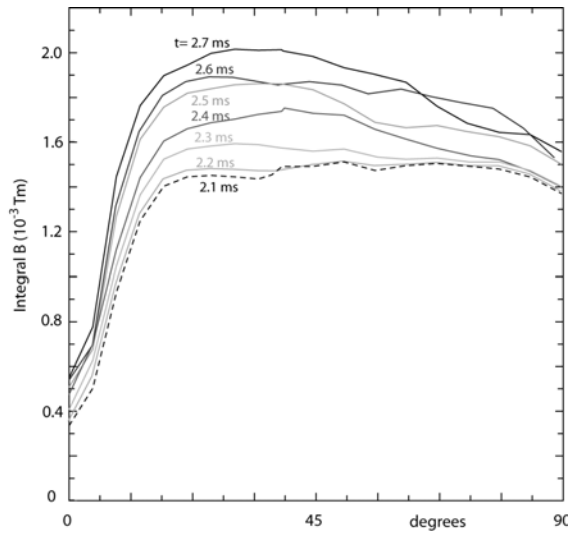


Figure 8. Modification of integral of B under solar wind compression. The later produces an increase of about 33%.

between the solar wind and the mini-magnetosphere. Reducing the solar wind density would mean that the simulations would have to be that much larger but with the same total force being exerted on the system. The value chosen here is sufficient to compress the mini-magnetosphere from its extended position detailed in Section 4.

The solar wind is imposed on the left hand boundary of the simulation system at $t = 1.7$ ms and arrives at the mini-magnetosphere at $t = 2.1$ ms. It is seen that arrival of the solar wind leads to the compression of the magnetic field for the two angles shown. The most important feature is that at now most regions forward in for the magnet have a falloff in the field strength close to R^{-1} . This change in slope is clear evidence that energy is being fed from the solar wind into the mini-magnetosphere via the compressional force that the solar wind exerts on the mini-magnetosphere. This is a critical result in that was conjectured in the original paper but not proven until now, and provides an explanation of the total energy balance in supporting a R^{-1} falloff in magnetic field across the bulk of the system.

Due to the reduced falloff in the magnetic field the value of the integral of B is increased by a factor of 33% as seen in Figure 8. Relative to the initial magnet this represents an increase of about 13 in the integral of B, and approaches the theoretical maximum discussed in Section 2. Two other features can be seen in Figure 7. First there is more turbulence in the system, particularly between the magnetopause and bow shock. This is not unexpected due to instabilities that arise

from the interpenetration of two plasmas. The other feature to note is that the incursion of the magnetic field perturbation from the solar wind interaction penetrates deeper into the mini-magnetosphere at higher elevations than at lower elevations. This is also seen in Figure 8 where the largest gains in the integral of B occur at mid latitudes.

The importance of the above latitudinal dependence is illustrated in Figure 9. The direction of the injected plasma stream is shown by blue arrows and is seen to be confined to near the equatorial plasma. The solar wind is clearly being deflected by this injected plasma as seen by its reduction in speed and redirection around the magnetopause. Penetration can occur only at high latitudes which also reinforces the compression of the injected plasma into the equatorial region. This deflection of plasma as measured by the difference in the integral of the momentum flux from in front and behind the mini-magnetosphere is found to be about 3 N which represents about a factor of 100 leverage in the momentum needed to sustain the mini-magnetosphere. This estimate is consistent with the original hall MHD simulations. The transfer region though is more clearly evident in the present work, occurring at mid- to high latitudes, as seen by following the velocity vectors.

Another way to see where the momentum transfer is occurring through the plasma Mach number (Figure 9b). Any region where the Mach number is greater than unity can clearly not transfer momentum onto the spacecraft. Thus, the plasma injection region confined to the spacecraft does not contribute to the momentum once it leaves the source and starts to expand the magnetic field. The equatorial magnetopause region is demarcated by stagnant (no net flow) plasma. This region of deflected plasma is held off in the equatorial plane from the magnet by the injected plasma. However, the cut in the x-z plane shows that this region of stagnant plasma maps to the magnet by the mid- to high latitude regions and it is here where the force is exerted on the magnet. This particle perspective is also consistent with the magnetic perspective where the magnetic perturbations from the solar wind move down the same region of latitude.

6. Summary and Conclusion

Multi-fluid simulations have been used to provide new insight into the physics of creating a mini-magnetosphere and the necessary properties required to successfully deflect energetic particles. It is shown that the injection of plasma leads to the formation of a diamagnetic cavity that leads to a very slow falloff

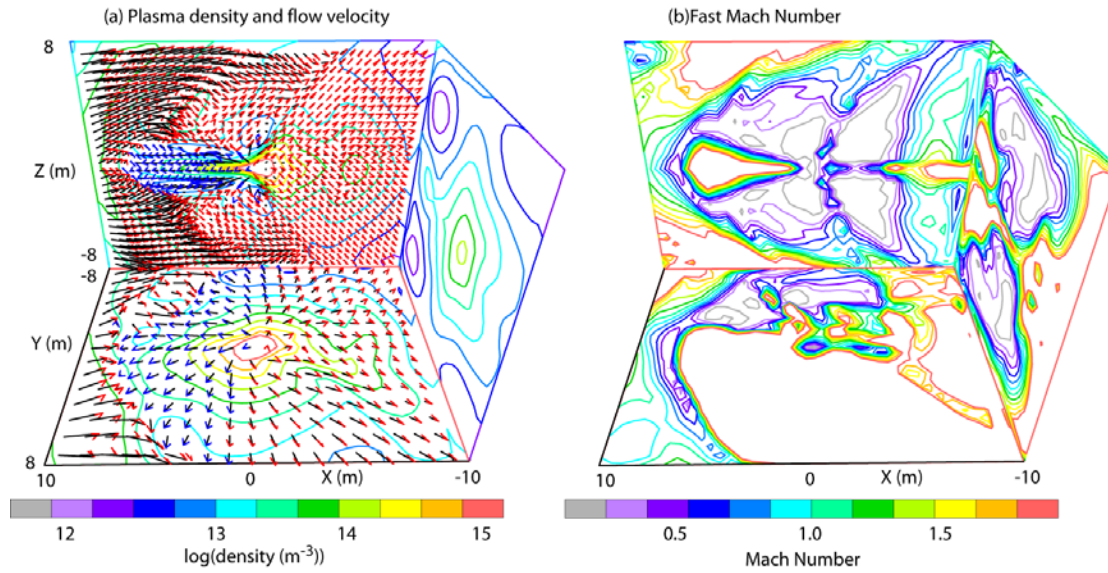


Figure 9. (a) Plasma flow speeds and density with blue and red arrows indicating flows in the direction of the plasma injection and solar wind respectively. (b) The plasma Mach number.

field with distance. Inflation alone without any other external plasma means though that the fall off in field is faster above the equatorial plane. Ion cyclotron effects produce a twisting of the magnetic field but the leverage of about 100:1 in thrust is still seen in the present simulations. Interaction with the solar wind leads to the compression of the system that enhances the magnetic energy density within the mini-magnetosphere and thereby increases its ability to deflect energetic particles. Thrust from the solar wind is conveyed to the magnet at mid- to high-latitudes through deflection of particles essentially in the cusp of the system and this deflection is associated with magnetic field perturbations close to the magnet.

In terms of shielding, the plasma injection means that the mini-magnetosphere can shield up to energies 200 times greater than the magnet by itself. The small system considered here of a 20 cm magnet and 1 kW was able to produce an integral of B alone a ray path of the order of 0.002 Tm. Enhances in this integral have of factors of about a factor of 4 have been achieved by increasing the magnet size by just a factor of 2. To attain GeV shielding the integral of B needs to be or order of 1 Tm. The above results for a simple interpolation (and ignoring economies of scale) can be achieved with plasma systems of the order of a few

100 kW, and as such makes it a viable candidate for human exploration.

7. References

- [1] Ip, W.-H., D. J. Williams, R. W. McEntire and B. Mauk, "Energetic ion sputtering effects at Ganymede", *Geophys. Res. Lett.*, **24**, 2631, 1997.
- [2] Fox, J. L. "Upper limit to the outflow of ions at Mars; Implications for atmospheric evolution", *Geophys. Res. Lett.*, **24**, 2901, 1997.
- [3] Winglee, R. M., J. Slough, T. Ziemba, and A. Goodson, "Mini-magnetospheric plasma propulsion: Tapping the energy of the solar wind for spacecraft propulsion", *J. Geophys. Res.*, **105**, 21,067, 2000.
- [4] Winglee, R. M., T. Ziemba, P. Euripides and J. Slough, "Computer Modeling of the Laboratory Testing of Mini-Magnetospheric Plasma Propulsion (M2P2)", *Proc. of 27th International Electric Propulsion Conference Proceedings*, **IEPC-01-200**, 2001.
- [5] Ziemba, T., R. M. Winglee, R. M. Winglee, and P. Euripides, "Parameterization of the Laboratory Performance of the Mini-Magnetospheric Plasma Propulsion (M2P2) Prototype", *Proc. of 27th International Electric Propulsion Conference*, **IEPC-01-201**, 2001.